

Supporting Information (ESI)

All-printed Organic Photodetectors with Metal Electrodes Enabled by One-step Solvent-mediated Transfer Printing Technology

Pengchao Zhou^{1,2#}, Jialu Gu^{2,3#}, Lei Fan¹, Jipeng Ma¹, Hong Lian^{2,3}, Wei Shi^{2,3*}, Bin Wei^{2,3*}

¹ *Affiliated Hospital of Jining Medical University, Jining, Shandong 273500, P. R. China*

² *School of Mechatronic Engineering and Automation, Shanghai University, Shanghai, Shanghai 200072, P. R. China*

³ *Key Laboratory of Advanced Display and System Applications, Ministry of Education, Shanghai University, Shanghai 200072, P. R. China*

co-first author, they contributed equally to this work.

*Corresponding authors:

Wei Shi, E-mail: shiwei@shu.edu.cn

Bin Wei, E-mail: bwei@shu.edu.cn

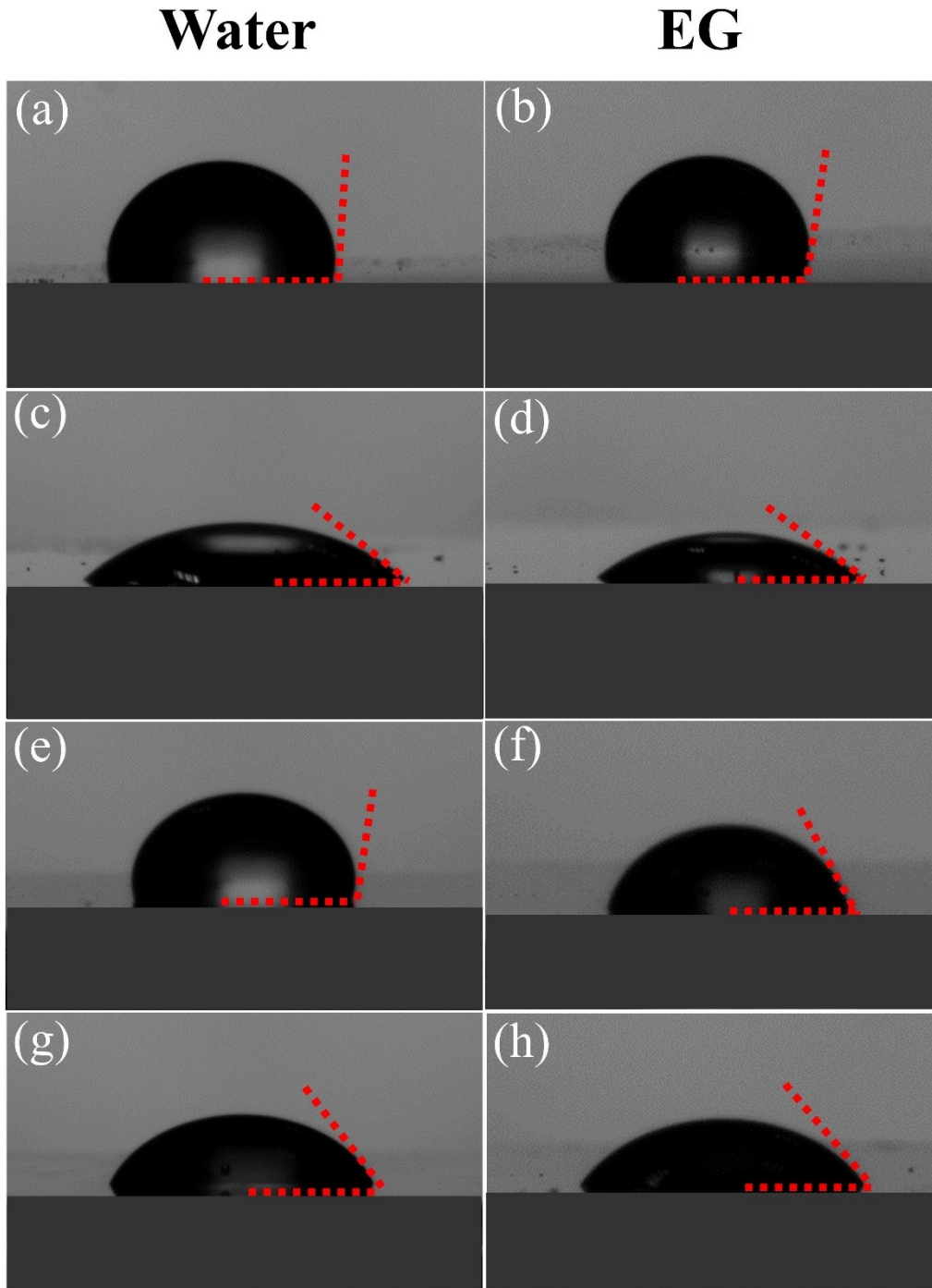


Figure S1. Contact angles of (a, b) PDMS, (c, d) ITO/Ag, (e, f) P3HT:PCBM, and (g, h) ITO films coated on glass substrates.

We measured the contact angles of water and ethylene glycol (EG) on different substrates, as shown in Figure 1. The corresponding polar and dispersive surface energy were obtained by the Owen-Wendt method based on the equation (1) and (2), as defined below:

$$\gamma_L(1 + \cos \theta) = 2\sqrt{\gamma_s^d \gamma_L^d} + 2\sqrt{\gamma_s^p \gamma_L^p} \quad (\text{S1})$$

$$\gamma_s = \gamma_s^d + \gamma_s^p \quad (\text{S2})$$

Where γ_L , γ_s^d , and γ_s^p represent the droplet surface energies, dispersive and polar components of water and EG, respectively. γ_s , γ_s^d , and γ_s^p is surface energies, dispersive and polar components of substrate, and θ is the contact angle of testing droplet on the corresponding substrate, respectively. The detailed records of θ and correspondingly calculated surface energies are presented in table 1. In light of the surface energy, interfacial energy between different materials can be determined according to the equation below:

$$\gamma_{A-B} = \gamma_A + \gamma_B - 4\left(\frac{\gamma_A^d \cdot \gamma_B^d}{\gamma_A^d + \gamma_B^d} + \frac{\gamma_A^p \cdot \gamma_B^p}{\gamma_A^p + \gamma_B^p}\right) \quad (\text{S3})$$

where γ_{A-B} represents the interfacial energy between material A and B, γ_A and γ_B represent the surface energy of material A and B, γ_A^d and γ_B^d are dispersion forces of material A and B, γ_A^p and γ_B^p are polarity forces of material A and sample B, respectively. The calculated interfacial energies between different layers are listed in Table S2.

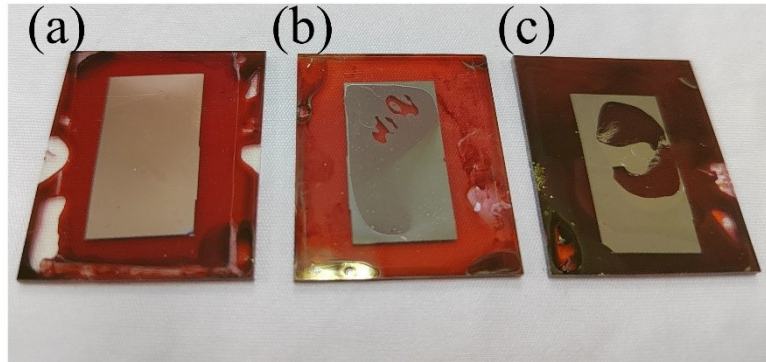


Figure S2. Transfer-printed Ag film at (a) 0, (b) 30, and (c) 60 minutes after the active layer solidification under the ambient temperature in the glove box.

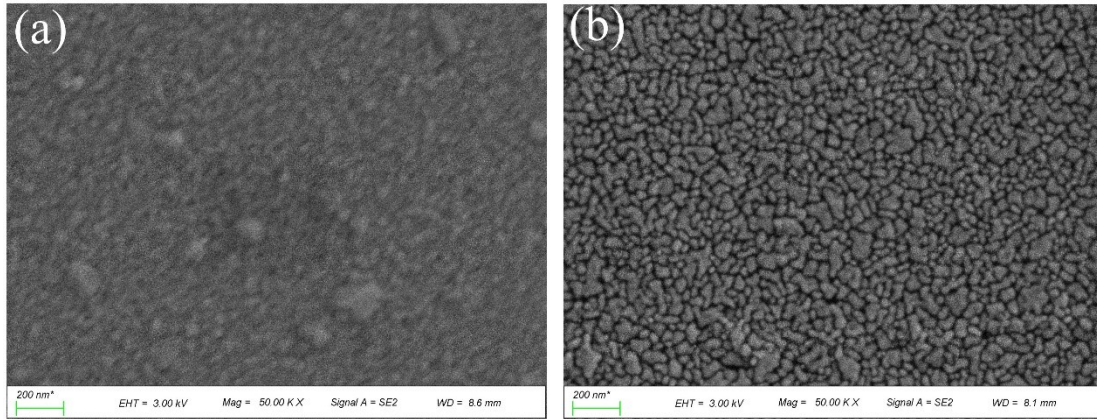


Figure S3. SEM images of the Ag film fabricated by (a) evaporation and (b) sTPT.

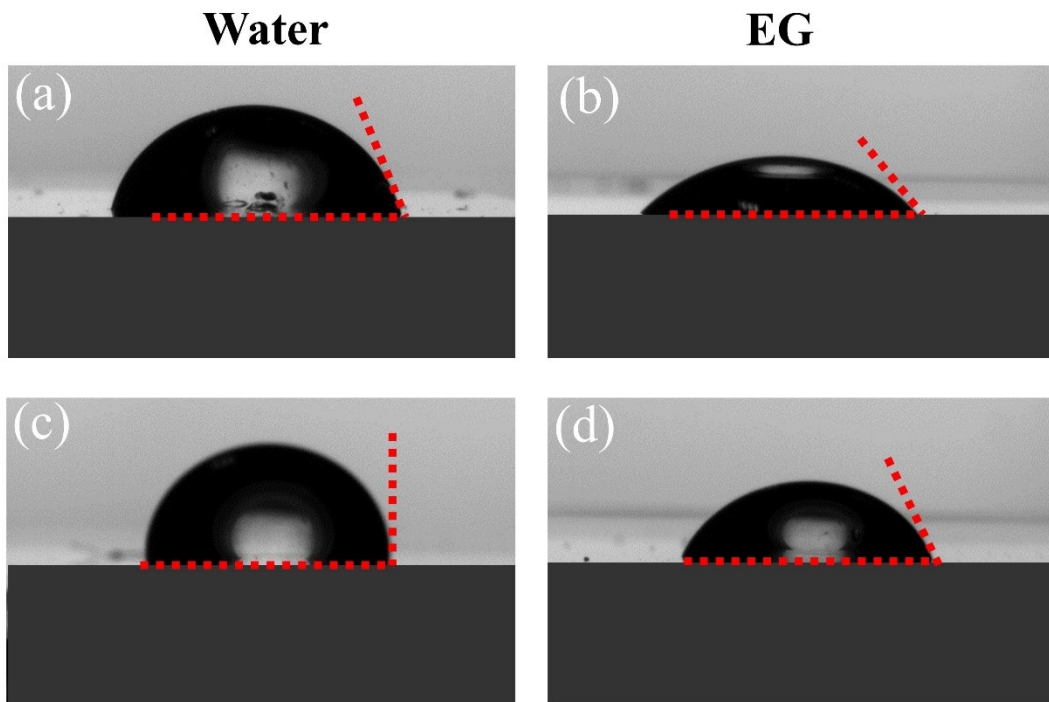


Figure S4. Contact angles of Ag films fabricated by (a, b) conventional evaporation and (c, d) sTPT.

If a surface is made up of two parts of different materials, the contact angle θ on such a composite surface can be expressed as follows:

$$\cos \theta = f_1 \cos \theta_1 + f_2 \cos \theta_2$$

Where f_1 and f_2 are the area fraction of those two parts, respectively. θ_1 and θ_2 are the corresponding intrinsic contact angles of a liquid droplet on those two materials.¹

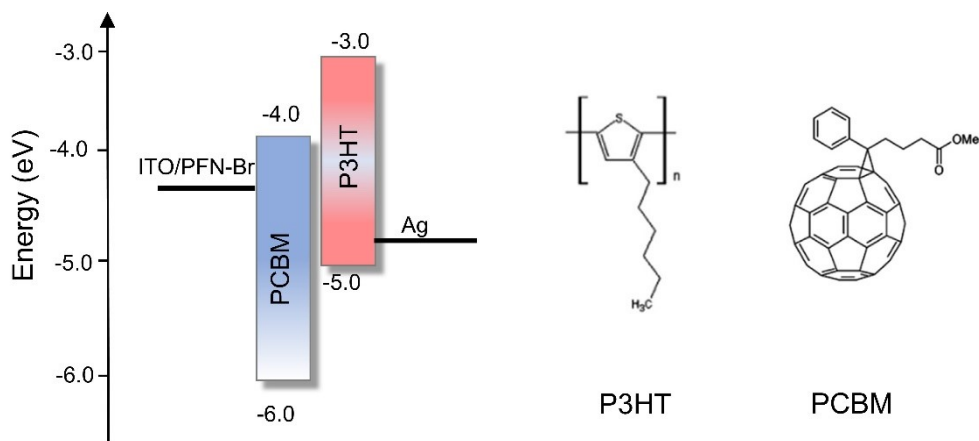


Figure S5. The energy level of individual layer used in OPDs and molecular structures of P3HT and PCBM.

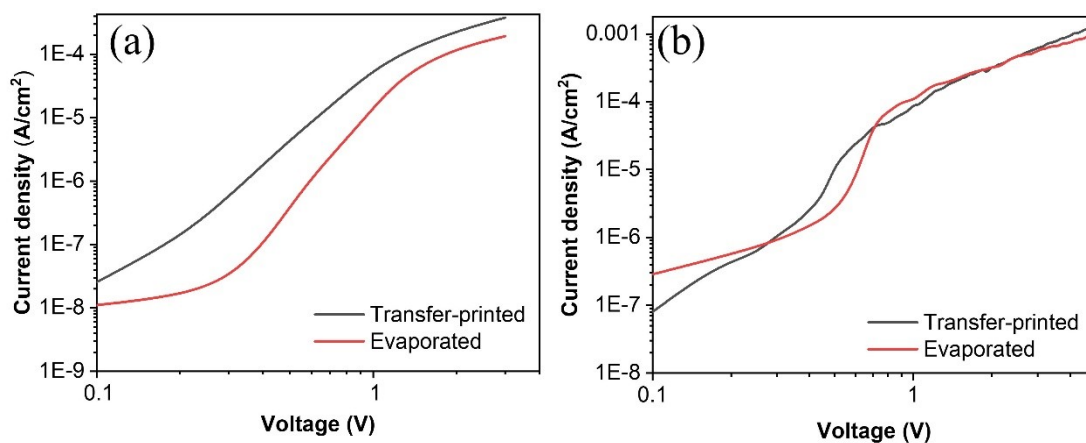


Figure S6. Dual log plots for $J-V$ curves of (a) electron only and (b) hole only devices with structures of ITO/PFN-Br/P3HT:PCBM/Ag and ITO/PEDOT:PSS/P3HT:PCBM/Ag, the Ag electrodes were fabricated by evaporation and sTPT.

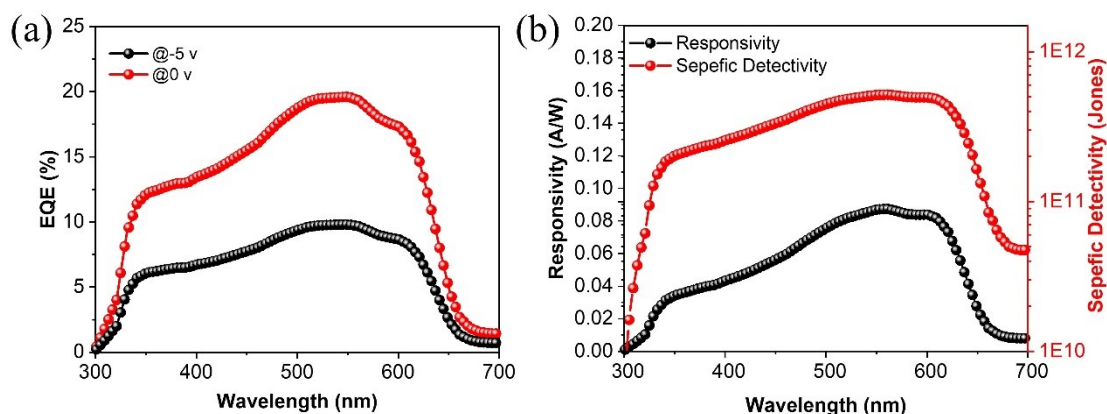


Figure S7. (a) EQE, (b) R and D^* curves of OPDs with transfer-printed Ag anodes under the bias of 0 and -5 V.

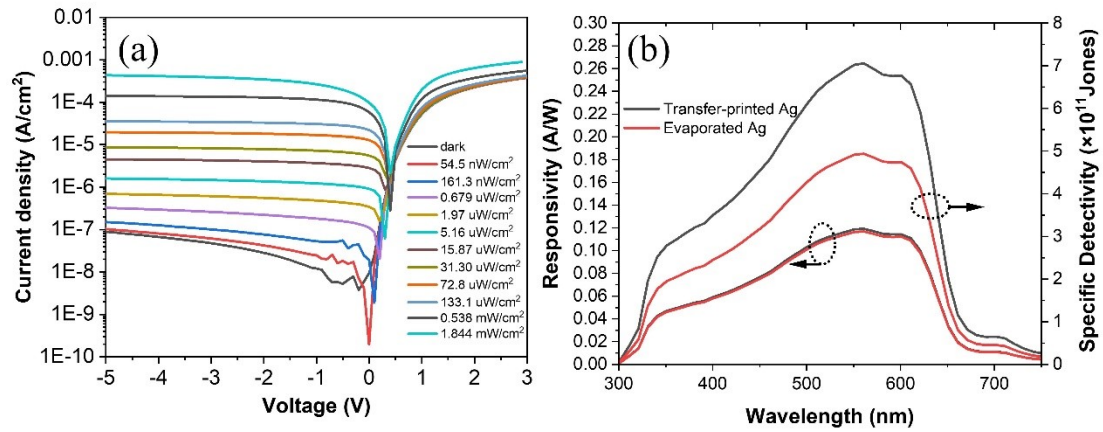


Figure S8. (a) J - V curves of OPDs under different illumination intensity for OPDs with transfer-printed Ag anodes. (b) R and D^* curves of OPDs with transfer-printed and evaporated Ag anodes under the bias of -5 V.

However, in Figure S8, estimating from the responsivity spectra at 540 nm, the R was 0.115 A/W, estimating from responsivity spectra, the J_{ph} may be about ~ 10 mA/cm², but the current density at -5 V was 1.09 mA/cm² under 100 mW/cm² in Figure 7b, we think may be ascribed to below reasons:

(1) Different incident spectra. The incident spectrum in Figure 7 was origin from Tungsten lamp with a band spectrum from 300nm to 3 μ m, with a light power density. But the actual power density within the corresponding spectral range (300 -750 nm) is far less than 100 mW/cm². The R in Figure S8 was calculated from EQE, and the EQE was calculated with a monochromatic light prepared through light filters.

(2) The sub-linear dependence at high light intensity. Although the OPD in our work with transfer-printed Ag anode had a better LDR , the LDR was observed with the highest incident density of 2 mW/cm², we believe that the sub-linear dependence would happen with the increase of incident light intensity and resulted in a decreased J_{ph} .

(3) Different devices. The OPD devices in Figure 7 were fabricated with another solvent of CB, and the OPD devices in Figure S8 were fabricate with the high-boiling point solvent—ODCB, hence varies for these two figures.

Table S1. Contact angles and surface energy of different films used in this work.

Substrate	Contact angle (degree)		Surface energy (mN/m)		
	water	EG	γ	γ^d	γ^p
P3HT:PCB M	101.4	74.8	25.822	25.278	0.544
PDMS	97.7	103.4	20.408	0.042	20.366
ITO	66.6	57.2	35.474	6.424	29.049
Ag (200 nm)	40.3	35.3	61.758	3.904	57.855

Table S2. The interfacial energy between two different materials.

Interface	γ (mN/m)
Ag/PDMS	21.746
Ag/P3HT:PCBM	71.904
Ag/ITO	10.164
PDMS/P3HT:PCB M	43.972
PDMS/ITO	7.827

Table S3. Contact angles and surface energy of Ag films fabricated by evaporation (E) and transfer printing technology (T) coated on the substrate of ITO/PFN-Br/P3HT:PCBM.

Film	Contact angle (degree)		Surface energy (mN/m)		
	water	EG	γ	γ^d	γ^p
Ag (E)	71.2	45.6	34.827	21.897	12.930

Ag (T)	88.6	63.2	27.764	23.972	3.792
--------	------	------	--------	--------	-------

Reference

1. Yong, J. L.; Chen, F.; Yang, Q.; Huo, J. L.; Hou, X., Superoleophobic surfaces. *ChSRv* **2017**, *46* (14), 4168-4217.